Journal of the European Ceramic Society 23 (2003) 707–713

www.elsevier.com/locate/jeurceramsoc

Microstructural and morphological analysis of pure and Ce-doped tin dioxide nanoparticles

A.P. Maciel[a], P.N. Lisboa-Filho[a], E.R. Leite[a,*], C.O. Paiva-Santos[b], W.H. Schreiner[c], Y. Maniette[b], E. Longo[a]

[a]*CMDMC-LIEC-DQ-UFSCar, São Carlos-SP, CEP 13565-905, Brazil*
[b]*IQ-UNESP-Araraquara-SP, CEP 14800-900, Brazil*
[c]*LSI-Depto. de Física-UFPR, Curitiba-PR, CEP 81531-990, Brazil*

Received 2 December 2001; received in revised form 14 May 2002; accepted 25 May 2002

Abstract

Structural and morphological studies in pure and Ce-doped tin dioxide nanoparticles with high stability against particle growth were performed in samples, obtained using the polymeric precursor method and prepared at different annealing temperatures. A Ce-rich surface layer was used to control the particle size and stabilize SnO_2 against particle growth. The formation of this segregated layer can contribute to a decreased surface energy, acting in the driving force, or reducing the surface mobility. Only the cassiterite SnO_2 phase was observed below 1000 °C and a secondary phase (CeO_2) was observed for the Ce-doped SnO_2 at temperatures higher than 1000 °C, when de-mixing process occurs. The evolution of crystallite size, microstrain and morphology of the nanoparticles with annealing temperatures was investigated by X-ray diffraction (XRD), associated to Rietveld refinements, X-ray photoelectron spectroscopy (XPS) and transmission electron microscopy (TEM).

Keywords: SnO_2; Powders-chemical preparation; X-ray methods; Precursors-organic

1. Introduction

The development of electrical and electronic devices with nanometric dimensions is a great challenge for technological applications.[1] The knowledge of microstructural properties of nanostructured semiconductor oxides has a fundamental role in the understanding and development of new electronic devices.

Several structural and scientific phenomena in Materials Science are directly related to particle size. In some cases, as in catalyst materials and gas sensor devices, it is desirable to produce materials with nanometric-scale structures to obtain and improve some specific properties.

In general, the reduction of the particle growth rate at high temperatures can be controlled using additives or, likewise, by different preparation methods, mainly the sol-gel for being a simple and low cost method.[2] Recently, we obtained nanostructured materials with high stability against particle growth using a metastable solid solution.[3]

The particle growth is dependent of the particle boundary motion.[4] The particle boundary velocity, V_b, may be expressed as,

$$V_b = M_b\ F_b \tag{1}$$

where V_b is proportional to the driving force for boundary migration, F_b, applied to it, and particle boundary mobility, M_b, which depends on the mechanism of diffusion. Thus, there are two distinct ways used for slow down the particle growth, one by the reduction of F_b and other by the reduction of particle boundary mobility.

Several authors controlled the particle growth through the formation of an external segregated oxide layer. It is known that the solute drag causes a decrease in particle mobility. The formation of this segregated layer can contribute to a decreased surface energy, acting on the driving force, or reducing the surface mobility. In either

* Corresponding author. Tel.: +55-16-260-8111; fax: +55-16-261-5215.
E-mail address: derl@power.ufscar.br (E.R. Leite).

0955-2219/02/$ - see front matter
PII: S0955-2219(02)00190-5

case, it contributes to decrease the particle boundary velocity.

In this paper, pure and Ce-doped tin dioxide nanoparticles were synthesized by the polymeric precursor method. We analyzed the influence of cerium oxide on the microstructure and segregation against particle growth. The evolution of the samples at different annealing temperatures was studied by using X-ray diffraction (XRD), X-ray photoelectron spectroscopy (XPS) and transmission electron microscopy (TEM).

2. Experimental

2.1. Preparation of nanoparticles

Pure and Ce-doped tin dioxide nanoparticles were prepared by the polymeric precursor method, based on the Pechini method,[5] using tin citrate aqueous solution, prepared from $SnCl_2.2H_2O$ (Mallinckrodt Baker, USA, purity >99.9%) and citric acid (E. Merck, Germany, purity >99.9%). The undoped tin polymer was obtained reacting the tin citrate with ethylene glycol, at a 1:1 mass ratio, in acid solution (HNO_3 conc.). In the case of the doped polymer, 5% in mol Ce^{4+}, using $Ce(NO_3).6H_2O$ (Sigma, purity >99.9%), was dissolved in the tin citrate solution, following the same procedure. In both cases the temperature was elevated up to approximately 120 °C to eliminate NO_x and heat-treated at 300 °C for 2 h for the pre-pyrolysis of the resin. The resulting polymer was treated at 400 °C for 4 h to allow for the complete oxidation of the organic precursor. Soon afterwards all materials were calcinated at several temperatures for 2 h to promote the crystallization of the SnO_2 phase. Fig. 1 shows the main steps required for the synthesis of the pure and Ce-doped tin dioxide nanoparticles.

2.2. Structural characterization

X-ray diffraction was carried out on a Siemens D-5000 instrument, in the Bragg θ-2θ geometry, equipped with a graphite monochromator and Cu K_α radiation (λ = 1.5418 Å), operating with voltage of 40 kV and emission current of 40 mA. Data were obtained in step times of 1.0 s and step sizes of 0.030° (2θ) from 20 to 60°. In the case of the routine for the Rietveld analysis, a scanning from 20 to 110° with step times of 8.0 s and step sizes of 0.020° was adapted.

The Rietveld refinement[6] was used for the crystal structure and microstructure analyses (crystallite size and microstrain), with the DBWS-9807a program (an

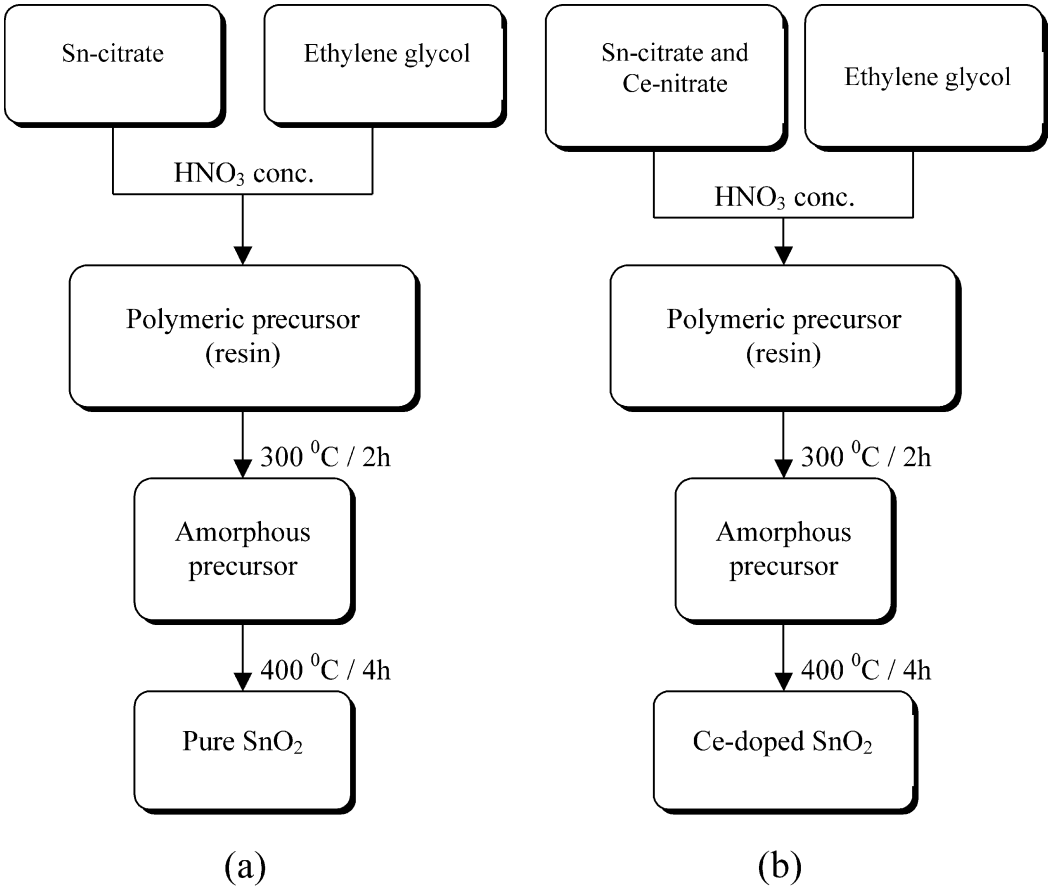

Fig. 1. The main steps for the synthesis of the pure (a) and Ce-doped (b) tin dioxide nanoparticles.

upgrade of the DBWS-9411 program).[7] The Thompson–Cox–Hastings function modified by Young (TCHZ)[8] was used for the diffraction profile fitting. The crystallite size and microstrain were computed using a model based on the Young–Desai method.[9,10] A tungsten carbide sample, previously characterized by the Rietveld method, was used as a standard to measure instrumental line broadening.

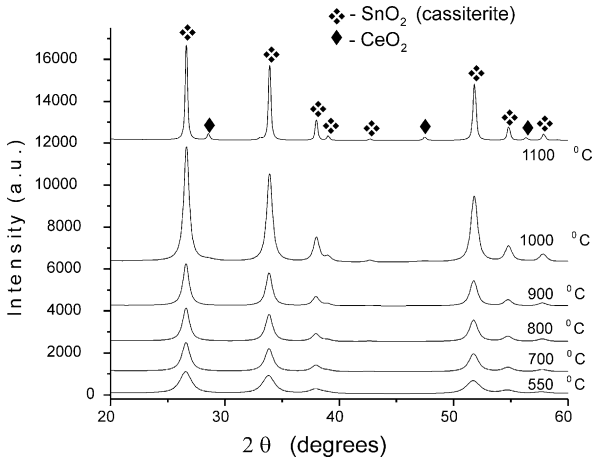

Fig. 2. X-ray diffractograms of the nanostructured Ce-doped SnO_2.

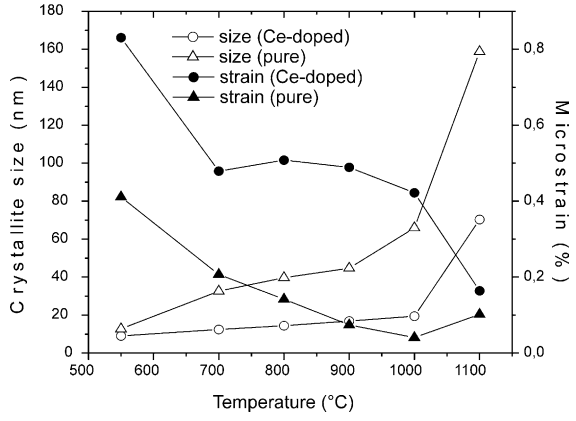

Fig. 3. Average crystallite size and microstrain as an function of heat treatment temperature, for the obtained nanoparticles.

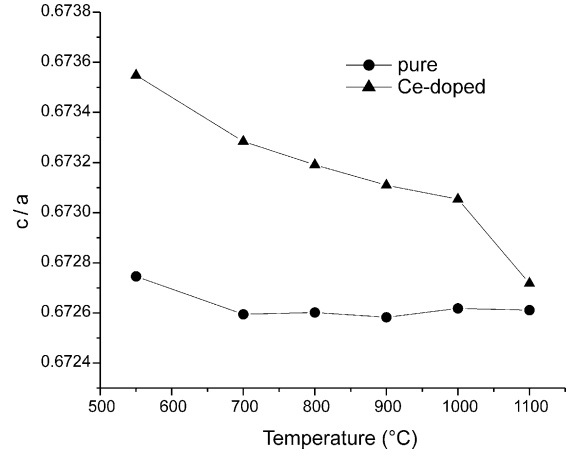

Fig. 4. The lattice parameter (c/a ratio) for pure and Ce-doped tin dioxide nanoparticles.

For the TEM/HRTEM analyses, a drop of the nanopowder suspension was ultrasonically dispersed in ethanol and deposited on a carbon-covered nickel grid. TEM observations were performed using a Philips CM 200 microscope operating at 200 kV. The X-ray photoelectron spectra were taken using a commercial VG ESCA 3000 system. The base pressure of the analysis chamber was in the low 10^{-1} mbar range. The spectra were collected using Mg K_α radiation and the overall energy resolution was about 0.8 eV. The concentrations of the surface elements were calculated using the system's database after subtracting the background counts.

3. Results and discussion

The X-ray diffractograms of the undoped SnO_2 displayed only the tetragonal rutile structure (cassiterite) for all the nanoparticles treated in the temperature range from 550 to 1100 °C. These results are in agreement with other works.[11,12] The results of X-ray diffraction, shown in Fig. 2, presented the tetragonal structure for Ce-doped SnO_2, but a second phase (CeO_2) was observed at temperatures above 1000 °C.

In both cases, pure and Ce-doped SnO_2 nanoparticles, the crystallite sizes increase with the increasing of the heat treatment temperature, while the microstrain and lattice parameter measurements (c/a ratio) decrease, as can be observed in Figs. 3 and 4, respectively. However, as already reported, the growth rate of the Ce-doped SnO_2 is smaller than the undoped material.[3]

The crystallite size (Fig. 2), in both cases, increases with increasing treatment temperature, though the

Table 1
Convergence parameters of the Rietveld refinement[a]

Sample	R_B	R_E (%)	R_P (%)	R_{wp} (%)	S
P550	1.56	5.71	5.88	7.82	1.37
P700	1.81	5.70	5.78	8.21	1.44
P800	1.54	5.71	5.70	8.37	1.46
P900	1.92	5.67	5.89	8.50	1.50
P1000	1.67	5.82	5.12	7.33	1.25
P1100	2.97	5.61	5.70	7.91	1.40
Ce550	3.01	8.36	7.64	9.91	1.18
Ce700	3.49	8.55	7.41	9.81	1.14
Ce800	3.43	10.23	7.76	10.23	1.20
Ce900	3.08	8.37	7.59	10.16	1.21
Ce1000	2.68	5.80	6.55	8.77	1.51
Ce1100	2.53	8.74	7.22	10.23	1.17

[a] The samples' codes are described as it follows: P = pure SnO_2; Ce = Ce-doped SnO_2 with 5% in mol of Ce and 550 – 1100 represent the treatment temperatures. The definitions for the R_B, R_E, R_P, R_{wp} and S were shown in Ref. 10.

Table 2
Results obtained by the Rietveld method for the microstructural characterization of the pure and Ce-doped SnO_2 nanopowders

Sample	Volume (Å^3)	Density (g/cm^3)	Cell parameters (Å)	
			a = b	c
P550	71.482	6.999	4.736406	3.186398
P700	71.502	6.997	4.737206	3.186219
P800	71.502	6.997	4.737185	3.186240
P900	71.502	6.997	4.737230	3.186178
P1000	71.497	6.998	4.737030	3.186211
P1100	71.502	6.997	4.737166	3.186270
Ce550	71.971	6.952	4.745285	3.196179
Ce700	71.861	6.962	4.743504	3.193726
Ce800	71.933	6.955	4.745295	3.194490
Ce900	71.857	6.963	4.743811	3.193105
Ce1000	71.792	6.969	4.742522	3.191971
Ce1100	71.578	6.990	4.738585	3.187732

increase for Ce-doped is slow. It exhibit a growth rate of $\sim 0.7\times10^{-2}$ nm/°C h in the 500–1000 °C range, while for the pure SnO_2 particles, at the same temperature range, the crystallite size displayed a faster increase ($\sim 4.8\times10^{-2}$ nm/°C h). These results show that Ce can be used to control particle size and stabilize SnO_2 against particle growth at that temperature range.

To understand the effect of dopant on particle growth control and microstructure, a Rietveld refinement study was performed in the pure and Ce-doped SnO_2, as a function of the heat treatment temperature. The convergence parameters of the Rietveld refinement[10] and the results for microstructural characterization of the pure and Ce-doped SnO_2 nanopowders are displayed in Tables 1 and 2, respectively. In Fig. 5 are presented the fittings that show the adjustment of the DRX curves for the Rietveld method.

Fig. 6 shows low magnification bright field (BF) transmission electron microscopy (TEM) images of the pure SnO_2 (Fig. 6a) and Ce-doped SnO_2 nanoparticles (Fig. 6b). The TEM reveals that the doped materials present smaller particle sizes than the pure material, but in both cases, uniform, well-crystallized nanoparticles can be observed. These results are similar to the results elsewhere[2,3] previously reported.

Fig. 7a shows the X-ray photoemission spectroscopy (XPS) results ([Ce]/[Sn]) for the Ce-doped SnO_2 samples prepared at different temperatures. The [Ce]/[Sn] con-

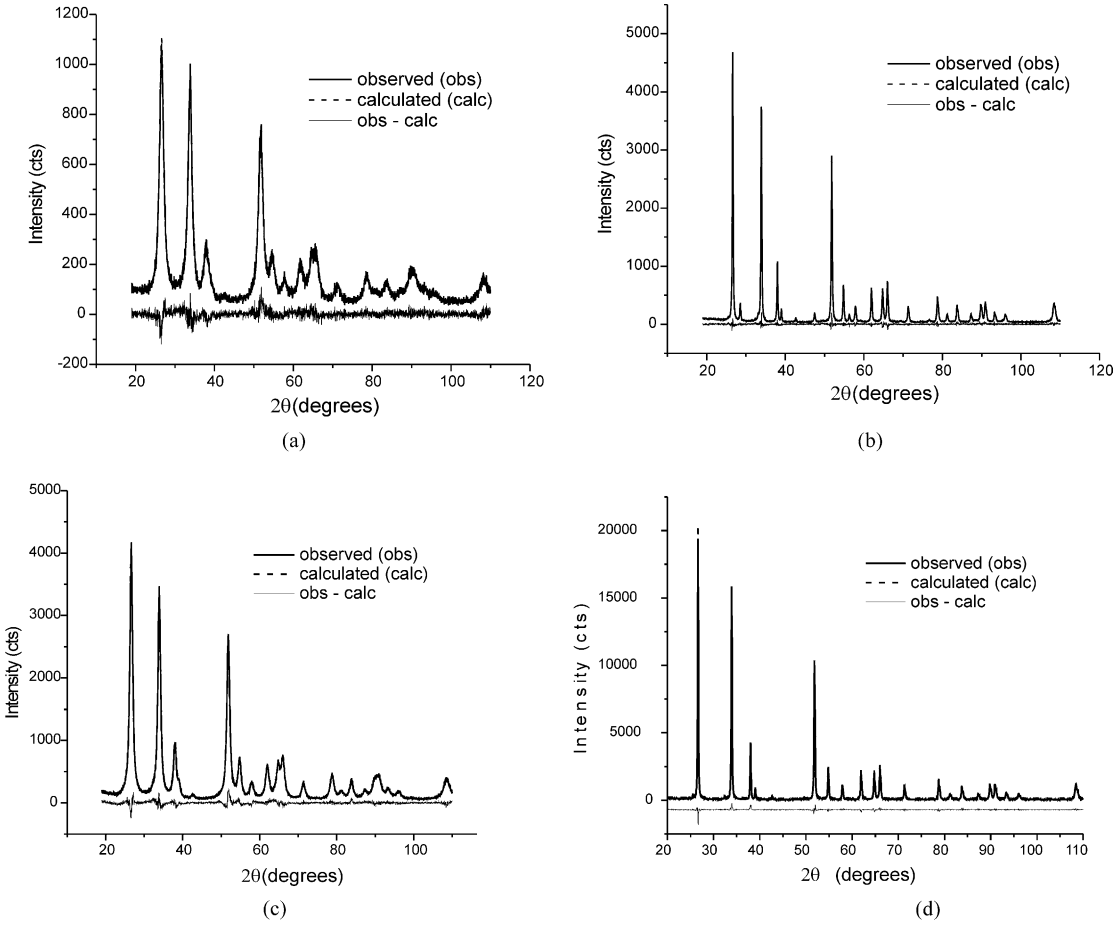

Fig. 5. Adjustment of the DRX curves for the Rietveld method: (a) Ce-doped heat-treated at 550 °C for 2 h, (b) Ce-doped heat-treated at 1100 °C for 2 h, (c) pure SnO_2 nanoparticles heat-treated at 550 °C for 2 h and (d) pure SnO_2 heat-treated at 1100 °C for 2 h.

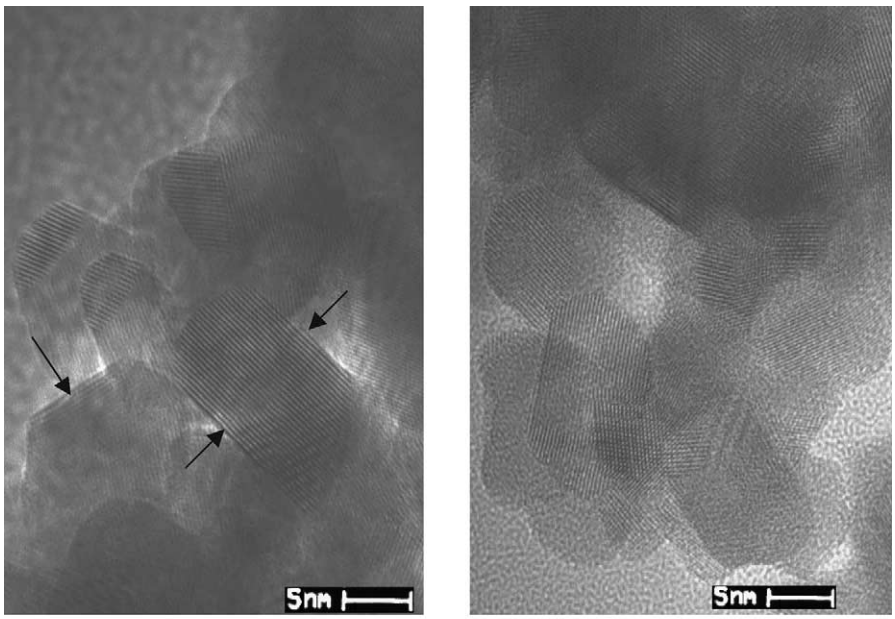

Fig. 6. Bright field (BF) transmission electron microscopy (TEM) images of pure (a) and Ce-doped SnO_2 nanoparticles (b). Material heat-treated at 550 °C for 2 h.

centration ratio grows up to 900 °C, after that it drastically decreases, as the annealing temperature rises.

It is clear, from the XPS results, that a surface rich in Ce cations is formed during the heat treatment ($T<900$ °C). However, for temperatures higher than 1000 °C, a de-mixing process ocurrs. These results are in agreement with the XRD data and show the formation of a segregation layer during the heat treatment.

Depero et al.[13] working with X-TiO_2 systems, where X=Al, Ga, Nb and Ta, observed a linear correlation between $<\varepsilon^2>^{1/2}$ (microstrain) and $1/<d>$, where $<d>$ is the average crystallite size. They showed, for rutile phase, the existence of a straight line passing by the origin. Based on this assumption: If

$$<\varepsilon^2>^{\frac{1}{2}}<d> \ \alpha \ \frac{1}{<d>}.$$

Consequently,

$$<Z_n^2>^{\frac{1}{2}} \alpha \ \frac{1}{<d>},$$

where $Z_n = n\,\varepsilon$ (n is the number of unit cells of the crystallite in a certain direction), and Z_n, in a single line Fourier analysis, one can assume the following gaussian distribution,

$$p(Z_n) = \frac{q}{\pi}\exp\left(-q^2 Z_n^2\right),$$

in the which the full width at the half maximum of the gaussian distribution of Z_n $(1/q)$ is inversely proportional to the average number of unit cells. This suggests that the microstrain existence is only due to the particle sizes.

In Fig. 8, can be observed a linear correlation between $<\varepsilon^2>^{1/2}$ and $1/<d>$ to Ce-doped nanoparticles. The inset in Fig. 8 shows a linear correlation between $<\varepsilon^2>^{1/2}.<d>$ and $1/<d>$ until 1000 °C, before the occurrence of the de-mixing process. This behavior was not observed for the pure SnO_2, thereby this indicates that the strain depends on the segregation and not on the average crystallite size.

These results suggest that a relaxation phenomenon occurs under the influence of temperature ($T<1000$ °C), driving the Ce from the inner lattice sites towards the

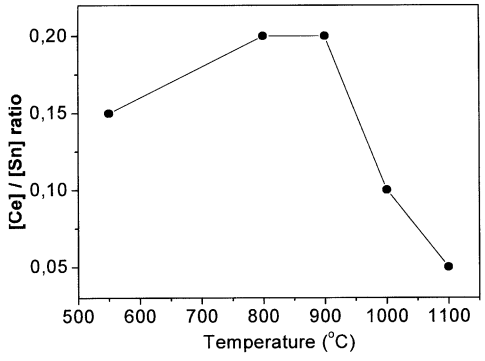

Fig. 7. XPS results, [Ce]/[Sn] ratio, for the Ce-doped SnO_2 nanoparticles.

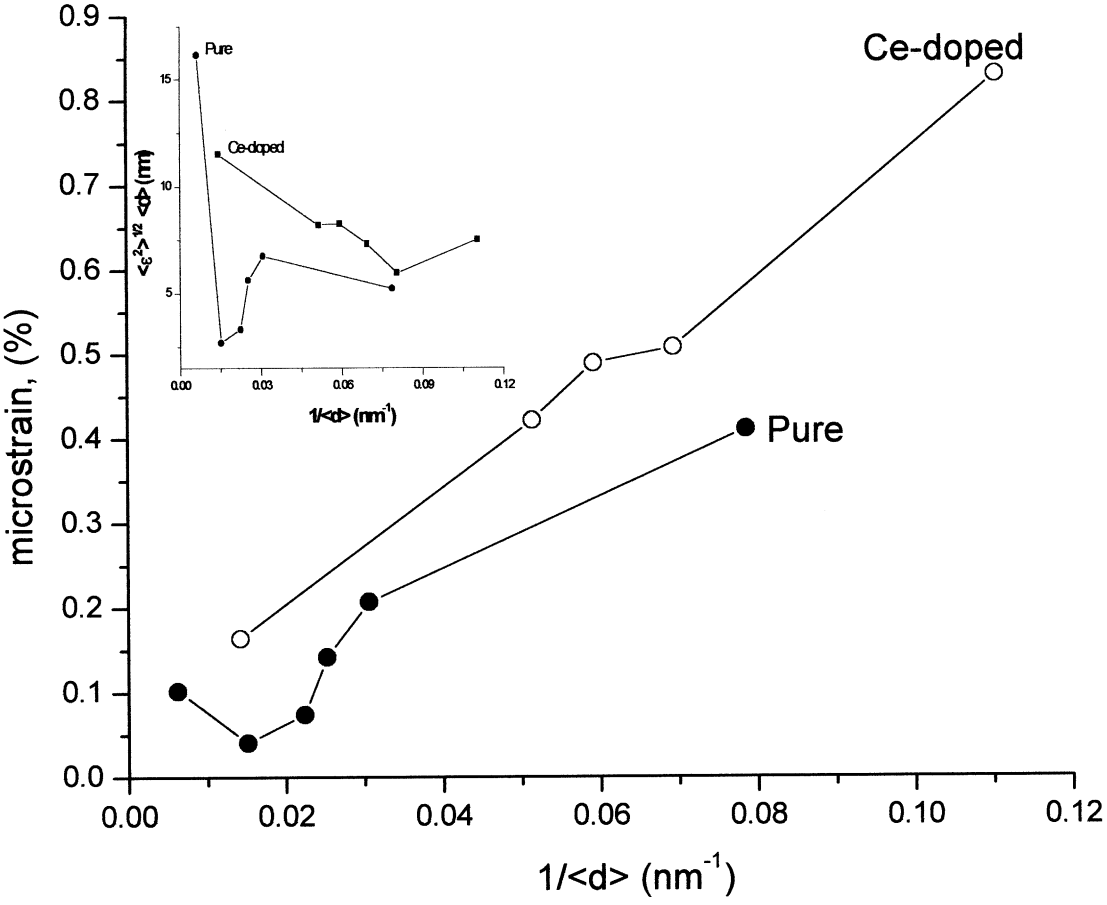

Fig. 8. Correlation between microstrain and average crystallite size for pure and Ce-doped tin dioxide nanoparticles.

surface and resulting in a nonhomogeneous solid solution whose surface is richer in the foreign cation, that next undergoes the dopant segregation. A secondary phase (CeO_2) was observed for the Ce-doped SnO_2 at temperatures starting from 1000 °C, while only the cassiterite SnO_2 phase was observed below 1000 °C. Thus, at $T \geqslant 1000$ °C, a de-mixing process occurs, resulting in a two-phase (SnO_2 and CeO_2) nanostructured material. Fig. 9 shows a qualitative model to explain the transformation that the Ce-doped SnO_2 nanoparticles undergo with the increase at the temperatures with the increase of the temperature, the Ce-segregation phenomenon is predominant up to 900 °C. For temperatures higher them 1000 °C, a de-mixing process occurs, resulting in a two phase materials.

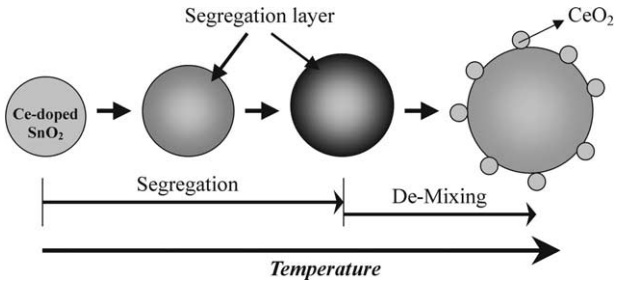

Fig. 9. The Ce-rich surface layer (segregation) formation followed by the de-mixing process.

Pure and Ce-doped tin dioxide nanoparticles, with high stability against particle growth were obtained by the polymeric precursor method. Their microstructural and morphological analyses demonstrate that their characteristics enable than for application as gas sensor devices.

4. Conclusions

This synthesis procedure of nanostructured tin dioxide powders promotes high thermal stability against particle growth at temperatures below 1000 °C. This low particle growth rate was obtained by the introduction of Ce particles into the SnO_2 lattice. The Ce cations move toward the particle surface, with increasing temperature, decreasing the particle growth velocity, thereby achieving to control the initial particle sizes below 20 nm at $T < 1000$ °C.

The cell volumes, microstrains and c/a ratio of the Ce-doped, for all treatment temperatures, are greater than the values of the pure SnO_2 nanoparticles. These facts indicate that Ce^{+4} (0.92 Å of diameter) is substituting Sn^{+4} (0.71 Å of diameter) in the crystallite. At high

temperatures, the c/a ratio and microstrain values of the Ce-doped are similar to those of the pure SnO_2 nanoparticles.

A Ce-rich surface layer is responsible for the particle growth inhibition and for the increase of the thermal stability of the nanometric particles against growth. The formation of this layer can contribute toward a decreased surface energy or a reduced surface mobility. In either case, it contributes to decrease the particle boundary velocity. This phenomenon is predominant up to 900 °C.

This methodology of preparation can be applied to modify the particle surface and then control the growth rate of the particles that takes places as the temperature rises. These nanostructured materials can be applied as gas sensor presenting an improved performance.

Acknowledgements

The authors acknowledge Brazilian support agencies, FAPESP, CNPq, FINEP and CAPES for financial support.

References

1. Andrievski, R. A. and Glezer, A. M., Size effects in properties of nanomaterials. *Scripta mater*, 2001, **44**, 1621–1624.
2. Leite, E. R., Weber, I. T., Longo, E. and Varela, J. A., A new method to control particle size and particle size distribution of SnO_2 nanoparticles for gas sensor applications. *Adv. Mater.*, 2000, **12**, 965–968.
3. Leite, E. R., Maciel, A.P., Weber, I. T., Lisboa-Filho, P. N., Longo, E., Paiva-Santos, C. O., Andrade, A. V. C., Paskocimas, C. A., Maniette, Y., and Schreiner, W. H. Development of metal oxide nanoparticles with high stability against particle growth using a metastable solid solution. *Adv. Mater.*, 2002, **14**, 905–908.
4. Chiang, Y. M., Birnie-III, D. P. and Kingery, W. D., *Physical Ceramics—Principles for Ceramic Science and Engineering*. John Wiley & Sons, New York, 1997.
5. Pechini, M., Method of preparing lead and alkaline earth titanates and niobates and coating method using the same to form a capacitor. Us Pat. No. 3330697, 1967.
6. Rietveld, H. M., A profile refinement method for nuclear and magnetic structures. *J. Appl. Cryst*, 1969, **10**, 65–71.
7. Young, R. A., Larson, A. C. and Paiva-Santos, C. O., *User's Guide to Program Dbws-9807 for Rietveld Analysis of X-Ray and Neutron Powder Diffraction Patterns*. School Of Physics, Georgia Inst. Of Technology, Atlanta, GA, USA, 1998.
8. Young, R. A. and Desai, P., Crystallite size and microstrian indicators in Rietveld refinament. *Arch. Nau. Mater.*, 1989, 71–90.
9. Paiva-Santos, C. O., Gouveia, H., Las, W. C. and Varela, J. A., Gauss-Lorentz size-strain broadenning and cell parameters analysis of Mn doped SnO_2 prepared by organic route. *Materials Structure*, 1999, **6**(2), 111–114.
10. Young, R. A. and Wiles, D. B., Profile shape functions in Rietveld refinements. *J. Appl. Cryst*, 1982, **15**, 430–438.
11. Leite, E. R., Cerri, J. A., Longo, E., Varela, J. A. and Paskocima, C. A., Sintering of ultrafine undoped SnO_2 powder. *J. Eur. Ceram. Soc.*, 2001, **21**, 669–675.
12. Weber, I. T., Andrade, R., Leite, E. R. and Longo, E., A study of the $SnO_2.Nb_2O_5$ system for an ethanol vapour sensor: a correlation between microstructure and sensor performance. *Sensors and Actuators B*, 2001, **72**, 180–183.
13. Depero, L.E, Sangaletti, L, Allieri, B., Bontemperi, E., Marino, A. and Zocci, M., Correlation between cystallite sizes and microstrains in TiO_2 nanopowders. *Journal Crystal Growth*, 1999, **198/199**, 516–520.